Phonon-libron dynamics of a commensurate molecular monolayer: (2 × 1) CO_2/NaCl(100)

C. Girardet, C. Ramseyer, P. N. M. Hoang, and S. Picaud
Laboratoire de Physique Moléculaire, UFR des Sciences et Techniques, Université de Franche—Comté, 25030 Besançon Cedex, France
(Received 27 January 1995)

The low-frequency dispersion curves of the (2 × 1) commensurate phase of CO_2 adsorbed on the ionic NaCl substrate are determined on the basis of potential calculations by including the dynamical coupling with the bulk and Rayleigh modes of the substrate and they are compared to recent inelastic helium atom scattering data. The analysis of the intensity of the resonance peaks in the time-of-flight scattering spectrum is done by considering (i) the influence of the polarization changes of the phonon-libron modes due to hybridization and avoided crossing; (ii) the presence of two types of monolayer domains; (iii) the mode selectivity of the experimental probe. The good consistency between calculations and experiments demonstrates the improved knowledge of interactions in such a physisorbed system, given the complexity and the richness of phenomena that have been interpreted.

I. INTRODUCTION

While photoemission and electron spectroscopies[1] have been currently used to probe the adsorption characteristics of physisorbed and chemisorbed species on metal surfaces, the vibrational modes of molecular adsorbates on single-crystal insulator substrates can be studied by nondestructive techniques such as Fourier transform infrared spectroscopy[2,3] (FTIRS) and inelastic helium atom scattering[4] (IHAS). In common, such methods emphasize the study of the influence of the adsorbate-substrate couplings on the adsorbate dynamics; they are, furthermore, quite complementary, since FTIRS gives information on the internal vibrations of the admolecules and IHAS probes external vibrations, which are, in general, too low in frequency to be detectable by the first technique.

The CO_2 monolayer adsorbed on NaCl(100) is one among the scarce systems to be recently studied by these two methods.[5] It has also been extensively investigated using low-energy electron diffraction[6] (LEED) and elastic He atom scattering,[7,8] and therefore it appears as an ideal candidate for a complete theoretical analysis. In contrast to FTIRS, the IHAS technique allows us to measure the frequency dispersion and to probe directly the coupling between the bulk and surface modes of the substrate and the translational and orientational modes of the monolayer. The phonon-libron dispersion curves associated with the collective low-energy modes of the CO_2 adlayer have been measured,[7] and the energy transfers between He projectiles and adlayer have been determined from time-of-flight (TOF) spectra transformed to energy distribution spectra.

In the course of our theoretical investigations on the CO_2-NaCl(100) system, we successively interpreted the monolayer structure[9] and the polarization infrared spectrum,[10] and performed preliminary calculations[11] on the adsorbate dynamics within the rigid substrate approximation. These various steps allowed us to test the pertinency of interaction potentials in explaining the value of the isosteric heat of adsorption, the molecular geometry on the ionic substrate, and the frequency shifts of the internal vibration modes induced by adsorption. Based on this preliminary information, the goal of the present paper is to perform detailed calculations of the monolayer dynamics including the couplings with the acoustic modes of the substrate. The frequency dispersion $\omega(\mathbf{q})$ for the adsorbate-substrate system is compared to data points issued from the analysis of the IHAS experiments.[7] The intensity of the resonance peaks in the TOF spectra can then be analyzed by considering the influence of hybridization on the mode polarization and the presence of monolayer domains. The ability of helium atoms for probing privileged polarization modes is also discussed through a comparison between calculated and experimental energy distribution spectra.

The outline of this paper is as follows. In Sec. II we give a brief report on the available information regarding the CO_2-NaCl(100) system. The theoretical backgrounds leading to the calculation of the dynamics and of the inelastic scattering cross section are presented in Sec. III. Numerical results and comparison with experiments are given in Sec. IV.

II. AVAILABLE INFORMATION

Both experiments issued from LEED,[6] polarization FTIRS,[12–16] and HAS,[7,8] and potential calculations[9] agree that the low temperature ($T \leq 80$ K) phase of the CO_2 layer adsorbed on single-crystal NaCl(100) surface has a stable (2 × 1) structure. The unit cell contains two molecules, which are tilted with respect to the normal to the surface by about 60° ± 4° (infrared results)

or 73° (calculations). The two molecular axes are mutually perpendicular ($\simeq 80°$ in both cases). The calculated value of the isosteric heat of adsorption (347 meV) is, furthermore, quite consistent with the thermodynamic data (369 ± 12 meV).[14]

Two different types of domains coexist at the NaCl surface, one labeled A with the glide plane parallel to the $\langle 110 \rangle$ direction and the other labeled B, which is rotated by 90°, having the glide plane in the $\langle 1\bar{1}0 \rangle$ direction. Two superimposed signals, therefore, occur[7] with intensity ratios proportional to the relative importance of domains A and B. The molar fraction of A and B is, however, not known. The infrared spectra exhibit pure vibrational Q branches, indicating that the orientational motions are mainly librational, as corroborated by calculations.[17] For the low-frequency modes of the monolayer alone, we thus expect 20 phonon dispersion curves corresponding to five translational + librational degrees of freedom for each of the two molecules in the unit cell and each domain A and B. Among the 20 expected dispersion branches, only eight have been observed[7] along the conventional $\overline{\Gamma X}$ azimuthal direction due, on one hand, to the symmetry introduced by the measurement technique and, on the other hand, to the superimposition of the layer signals with the bulk phonon modes of the substrate. This latter feature limits the detection of branches with energies lower than 10 meV.

The TOF spectra have been recorded[5,7] at 30 K for an incident wave vector $k_i = 5.17$ Å^{-1} and by varying the angle of incidence θ_i of the helium beam between 43° and 57° in order to follow vibrational modes in a very restricted number of reciprocal zones (one or two Brillouin zones). The measured energy resolution is about 0.35 meV. The interpretation of the scattering spectra must therefore take into account these experimental conditions, which imply the following consequences: (i) at such a temperature mainly the energy loss side caused by one-phonon processes can be observed, (ii) the measured momentum transfers are transformed to phonons belonging to the first Brillouin zone and a special care must be brought to the behavior of the resonance peak intensities with the Brillouin zone number, and (iii) the instrumental resolution prevents the detection of close frequency vibrational modes with different polarizations.

The identification of the monolayer modes has been discussed on the basis[5,7] of a normal mode analysis at the $\overline{\Gamma}$ point of the first Brillouin zone under the constraints of equivalent adsorption sites for the two molecules and of the particular sensitivity of HAS in detecting adsorbate motions perpendicular to the surface. Some dispersion curves were qualitatively assigned to hindered molecular collective translations or rotations but the complexity of the diagram did not allow a complete interpretation without the help of a lattice dynamical calculation. Such calculations have been recently performed[11] on the basis of semiclassical interaction potentials. Although the model used was oversimplified because we assume the substrate to be rigid and we limit our analysis to the mode frequency and to their mutual polarization, we find a semiquantitative agreement with the dispersion data. Among the 20 dispersion branches, four have a quasiacoustical behavior with an energy less than 5 meV, while the remaining 16 curves correspond to more or less dispersive optical branches ranging between 5 and 14 meV.

The present calculations are much more general, since most of the weaknesses in the previous work have been removed, and they allow a direct quantitative comparison between the experimental and calculated scattering spectra. However, we extensively use the parts of information given in Ref. 11 and relative to (i) the interaction potential between the adsorbate and the substrate and between the adsorbate molecules, (ii) the equilibrium geometries of the adsorbate, and (iii) the calculation of the effective force constants experienced by the admolecules.

III. THEORETICAL BACKGROUNDS

A. Coupled dynamics for the adsorbate-substrate system

1. *Interaction, equilibrium, and potential well shape*

The potentials V_{MS} and V_{MM} characterizing respectively the monolayer-substrate and intramonolayer interactions are mainly described by pairwise atom-atom dispersion-repulsion ($\simeq 40\%$ of the total potential) and by electrostatic ($\simeq 50\%$ of the potential) contributions. The dominant contributions are the substrate charge-molecular quadrupole interactions for V_{MS} and the quadrupolar interactions for V_{MM}. The other contributions (higher-order electrostatic terms, induction and substrate mediated contributions, corrections for surface relaxation and rumpling, etc.) remain small ($\simeq 10\%$) and within the present inaccuracy on the potential coefficient determination.[9]

The monolayer equilibrium configuration calculated at 0 K by minimizing the total potential $V_{MS} + V_{MM}$ and by assuming the substrate to be rigid is shown in Fig.1.

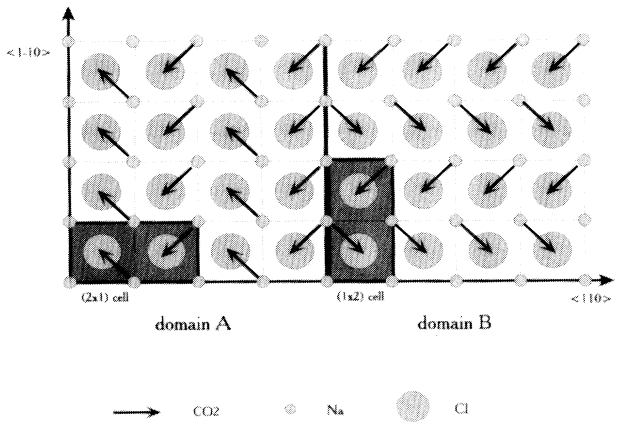

FIG. 1. Geometry of the (2×1) commensurate CO_2 monolayer adsorbed on NaCl(100). The two unit cells associated with domains A (left) and B (right) are represented by dark rectangles. The arrows indicate that the molecular axes are tilted upwards.

The (2×1) unit cell with area $2a^2$ ($a = 3.96$ Å) contains two inequivalently adsorbed CO_2 molecules with the axis configuration given in Sec. II. The translational and orientational potential wells are deep and sharp, and small linear or angular oscillations around the equilibrium are expected[17] for the CO_2 admolecules. A numerical fit of the potential shape around the equilibrium is performed; this allows us to calculate the components $\tilde{\phi}_{\alpha\beta}$ of the effective force constant tensor experienced by a molecular pair embedded in the layer.[11] Such a procedure limits the series expansion of the potential to the quadratic contribution, but it introduces, through the effective values of $\tilde{\phi}_{\alpha\beta}$, the influence of higher-order terms in the series.

2. Lagrangian

The Lagrangian for the effective harmonic monolayer is written as

$$L_M = \frac{1}{2}\sum_{\alpha\ell s}\left[A_\alpha\left|\dot{u}_\alpha\binom{\ell}{s}\right|^2 - \sum_{\beta\ell' s'}\tilde{\phi}_{\alpha\beta}\binom{\ell\ \ell'}{s s'}u_\alpha\binom{\ell}{s}u_\beta\binom{\ell'}{s'}\right], \quad (1)$$

where $u_\alpha\binom{\ell}{s}$ defines the linear ($\alpha = x, y, z$) or angular ($\alpha = \theta, \phi$) displacement of the sth CO_2 molecule belonging to the ℓth (2×1) unit cell. A_α characterizes the molecular mass m ($\alpha = x, y, z$) or the momentum of inertia I ($\alpha = \theta$) or $I\sin^2\theta$ ($\alpha = \phi$) of CO_2.

To define the Lagrangian of the substrate, we consider that it behaves as an isotropic elastic continuum. The continuum hypothesis is justified for this study, since the energy of the external modes in the monolayer does not exceed 14 meV. Indeed, due to the stiffness of the potential between the substrate ions, on one hand, the optical substrate modes have energies too large to hybridize with the layer modes, and, on the other hand, the acoustic substrate modes have a quasilinear behavior in the energy range of the layer branches. Moreover, the anisotropy coefficient for the acoustical substrate modes of NaCl is sufficiently close to unity ($K \simeq 0.8$) to expect[18] that the isotropic assumption works quite well. The expression of the Lagrangian for the elastic substrate is therefore given by:[19]

$$L_S = \frac{1}{2}\sum_\gamma \int d\mathbf{r}\left[\rho|\dot{u}'_\gamma(\mathbf{r})|^2 - \sum_{\epsilon\lambda\mu}\int d\mathbf{r}'\Lambda_{\gamma\epsilon\lambda\mu}\nabla_\epsilon u'_\gamma(\mathbf{r})\nabla_\mu u'_\lambda(\mathbf{r}')\right], \quad (2)$$

where the integral is over the substrate volume with homogeneous matter density ρ. The small continuum volume element $d\mathbf{r}$ at the position $\mathbf{r}$ is displaced by $\mathbf{u}'(\mathbf{r})$ with respect to the equilibrium; $\gamma, \epsilon, \lambda$, and μ correspond to the variables x, y, and z and the elastic modulus tensor $\underline{\Lambda}$ is the usual four rank tensor for an isotropic homogeneous elastic continuum characterized only by the longitudinal c_ℓ and transverse c_t sound velocities. Note that $\underline{\Lambda}$ appears in fact as an effective tensor, which takes into account the static influence of the monolayer on the substrate dynamics. However the adsorbate-substrate interactions are weak when compared to the stiffness of the intrasubstrate bonds, and the modifications induced by the monolayer adsorption on the tensor $\underline{\Lambda}$ are negligible.[20]

The dynamical coupling between the substrate and the layer is bilinear with respect to the motions $\mathbf{u}\binom{\ell}{s}$ of the admolecules and $\mathbf{u}'(\mathbf{r})$ of the volume element of the substrate. This Lagrangian takes the form

$$L_C = \sum_{\alpha\ell s}\sum_\gamma \int d\mathbf{r}\,\chi_{\alpha\gamma}(\ell s, \mathbf{r})u_\alpha\binom{\ell}{s}u'_\gamma(\mathbf{r}), \quad (3)$$

which can be easily deduced from the series expansion of the potential V_{MS} up to the quadratic order. To calculate the force constant tensor $\underline{\chi}$, we assume[21] that the substrate volume element is a parallelepipedal box with the same area as the (2×1) unit cell and formed by two parallel planes, each containing two Na and two Cl ions. The components $\chi_{\alpha\gamma}$ are mean values of the pairwise force constants between a molecule and every ion in the volume element, and they are referred to the center of the box. Such a method allows us to conciliate the continuum description of the substrate dynamics with the discrete representation of the monolayer and of the adsorbate/substrate interactions.

The total Lagrangian $L = L_M + L_S + L_C$ is then used to determine the coupled equations of motion for the total system.

3. Equations of motion

For the adsorbate and substrate displacements we assume[21,22] Bloch waves with $\mathbf{q}$ wave vector inside the plane (x, y). The monolayer dynamics for the sth ($s = 1, 2$) molecule in the origin unit cell is written as

$$\sum_{\beta s'}(d_{\alpha\beta}(s, s', \mathbf{q}) - \omega^2\delta_{\alpha\beta}\delta_{ss'})u_\beta(s') = \sum_\gamma \int dz\ \ \Gamma^2_{\alpha\gamma}(s, z, \mathbf{q})\ u'_\gamma(z). \quad (4)$$

$\underline{d}$ is a ten-rank matrix associated with the translational and librational dynamics of the adsorbate. The linear coupling of the layer with the substrate motions occurring in Eq. (3) is redefined as $\underline{\Gamma}^2$, which is homogeneous to a square frequency and depends on the depth of the volume element with respect to the substrate surface.

In a similar way, the equation of motion for the elastic continuum coupled to the monolayer is expressed for the small volume element located at z, as

$$\sum_\epsilon(K_{\gamma\epsilon}(\mathbf{q}) - \omega^2\delta_{\gamma\epsilon})u'_\epsilon(z) = \sum_{s,\alpha}\Delta^2_{\gamma\alpha}(s, z, \mathbf{q})u_\alpha(s). \quad (5)$$

$\underline{K}$ is the usual third rank Green-Christoffel propagation matrix[19] for the acoustic waves in the elastic continuum

defined through the longitudinal and transverse sound velocities. As already mentioned, the static influence of the adlayer is disregarded, and therefore $\underline{K}$ does not depend on z. The term $\underline{\Delta}^2$ homogeneous to a square frequency characterizes the coupling of the substrate volume element at depth z with the whole layer motions [cf. Eq. (3)]. $\underline{\Delta}^2$ appears as a (3×10) rectangular matrix, while $\underline{\Gamma}^2$ in Eq. (4) has the (10×3) dimension.

Equation (5) is formally solved to determine $u'_\epsilon(z)$, which is then substituted into Eq. (4)

$$\sum_{\beta s'}\left(d_{\alpha\beta}(s,s',\mathbf{q}) - \omega^2\delta_{\alpha\beta}\delta_{ss'} - \sum_s\sum_{\gamma\epsilon}\int_{-\infty}^{0} dz\ \Gamma^2_{\alpha\gamma}(s,z,\mathbf{q})G^{ss'}_{\gamma\epsilon}(\omega^2,\mathbf{q})\Delta^2_{\epsilon\beta}(s',z,\mathbf{q})\right)u_\beta(s') = 0. \tag{6}$$

Equation (6) represents a system of ten coupled equations for the layer dynamics themselves coupled to the substrate. The integral is over the substrate depth z, which is considered negative inside the crystal. The Green tensor $\underline{G}$ is the inverse of the dynamical Christoffel matrix $(\underline{K} - \omega^2\underline{I})$ in Eq. (5), and it contains in its poles all the dynamical information on the substrate. These poles correspond to the acoustic bulk mode frequencies and to the Rayleigh frequencies, which are obtained by applying the zero stress conditions at the substrate surface ($z = 0$). Indeed after tedious analytical calculations, the components of the Green tensor $\underline{G}$ can be written as

$$G_{\alpha\beta} = \frac{G^0_{\alpha\beta}(\omega^2,\mathbf{q})}{M(\omega^2,\mathbf{q})}, \tag{7}$$

where $\underline{G}^0$ does not contain poles that only appear as the zeros of the M function defined as

$$M(\omega^2,\mathbf{q}) = \left(q^2 - \frac{\omega^2}{c_t^2}\right)^4\left(q^2 - \frac{\omega^2}{c_\ell^2}\right)^2\left[\left(2q^2 - \frac{\omega^2}{c_t^2}\right)^2 - 4q^2\sqrt{\left(q^2 - \frac{\omega^2}{c_t^2}\right)\left(q^2 - \frac{\omega^2}{c_\ell^2}\right)}\right]. \tag{8}$$

The first two terms in the right-hand side of Eq. (8) correspond to the bulk frequencies, whereas the term in the brackets gives the usual Rayleigh mode,[19] since the static influence of the layer on the substrate has been neglected.

The solutions of Eq. (6) cannot be obtained from a conventional diagonalization of the dynamical matrix, since the square frequency ω^2 appears in the diagonal as well as in the nondiagonal terms, through the $\underline{G}$ function occurring in the coupling terms. When the couplings $\underline{\Gamma}^2$ and $\underline{\Delta}^2$ vanish, Eqs. (4) and (5) can be solved in a separate way and they give, on one hand, the dispersion curves of the monolayer above the rigid substrate and, on the other hand, the bulk and Rayleigh modes of the elastic continuum. Hybridizations and avoided crossings of the dispersion curves between the substrate and adsorbate modes occur through the couplings $\underline{\Gamma}^2 \neq 0$ and $\underline{\Delta}^2 \neq 0$ in Eq. (6). Note again that the displacements in this latter equation are associated to the monolayer only, those describing the motions of the substrate volume element are determined from Eq. (5) as functions of the monolayer displacements, as

$$u'_\gamma(z) = \sum_{s\beta\epsilon} G_{\gamma\epsilon}(\omega^2,\mathbf{q})\Delta^2_{\epsilon\beta}(s,z,\mathbf{q})u_\beta(s). \tag{9}$$

B. Inelastic scattering cross section

Many theoretical calculations[23–25] have been devoted to the determination of the collisional process between thermal helium atoms and a surface. In this section, we do not calculate the matrix elements describing the interaction between the probe projectile and the surface, but we limit our discussion to the analysis of the energy and intensity of the resonance peaks in the TOF scattering spectrum transformed to energy transfer distribution spectra for the phonons-librons of the monolayer. The differential cross section per scattered energy unit E_f and solid angle unit Ω_f is usually defined as[24,25]

$$\frac{d^2\sigma}{dE_f d\Omega_f} \propto \sum_j\sum_{\mathbf{g}}\sum_{ss'} e^{i(\mathbf{Q}_\parallel - \mathbf{g})\cdot[\mathbf{R}_\parallel(s') - \mathbf{R}_\parallel(s)]} \times\left[\beta^\parallel_{ss'}(\mathbf{Q}_\parallel - \mathbf{g})\sum_{\mathbf{G}} P^\parallel_{ss'}(\mathbf{Q}_\parallel - \mathbf{G} - \mathbf{g}, j) + \beta^\perp_{ss'}(\mathbf{Q}_\parallel - \mathbf{g})\sum_{\mathbf{G}} P^\perp_{ss'}(\mathbf{Q}_\parallel - \mathbf{G} - \mathbf{g}, j)\right]F_j(\mathbf{Q}_\parallel - \mathbf{G} - \mathbf{g}, \omega). \tag{10}$$

$\hbar\mathbf{Q}_\parallel$ characterizes the parallel momentum transfer between the probe and the adsorbate and $\mathbf{g}$ and $\mathbf{G}$ are the two-dimensional (2D) reciprocal primitive translation vectors connected to the (2×1) unit cell and defined by (g_1 and g_2 integers)

$$\mathbf{g} = \frac{2\pi}{a}\left(\frac{g_1}{2}\mathbf{x} + g_2\mathbf{y}\right). \tag{11}$$

$j = 1, \ldots, 13$ corresponds to the ten monolayer branches and to the three (bulk + Rayleigh modes) substrate

branches; $\mathbf{R}_{\|}$ defines the equilibrium position of the sth molecule in the cell.

The functions $P_{ss'}^{\|,\perp}$, characterize the relative orientation of the 3D transfer momentum $\hbar\mathbf{Q}$ ($\hbar\mathbf{Q}_{\|}, \hbar\mathbf{Q}_{\perp}$) with respect to the adsorbate-substrate displacements defined by the supervector $\mathbf{W} = \binom{\mathbf{u}}{\mathbf{u}'}$ [cf. Eqs. (6) and (9)]. They are expressed as

$$P_{ss'} = \left[\mathbf{Q}\cdot\mathbf{W}^{*}(s', \mathbf{Q}_{\|} - \mathbf{G} - \mathbf{g}, j)\right] \times \left[\mathbf{Q}\cdot\mathbf{W}(s, \mathbf{Q}_{\|} - \mathbf{G} - \mathbf{g}, j)\right]. \quad (12)$$

The whole information on the collisional process between the probe He atom and the adsorbate is contained in the functions $\beta_{ss'}^{\|,\perp}$, which are generally determined by close coupling, perturbation series or wave packet propagation techniques.[25] Two asymptotic situations S_1 and S_2 are considered here, based on the results of the approximate corrugated hard wall model:[23] (i) the first, S_1, consists in neglecting the parallel component $\beta^{\|}$ in agreement with the rule that He atoms are mostly sensitive to perpendicular motions of the adsorbate and substrate ($\beta^{\|} = 0; \beta^{\perp} = 1$); (ii) in the second situation, S_2, we assume an equal weight for the parallel and perpendicular components ($\beta^{\|} = \beta^{\perp} = \frac{1}{2}$). In every situation $\beta^{\|,\perp}$ are assumed to be independent of the wave vector.

The function F_j in Eq. (10) describes the temperature dependence and time evolution of the monolayer-substrate motions through the correlation functions $\langle\mathbf{W}(t)\mathbf{W}(0)\rangle$. Within the effective harmonic approximation for the adsorbate dynamics, the intrinsic broadening of the resonance peaks is neglected and F_j is simply written in terms of the Bose function $n_{\mathbf{q}_j}(T)$ associated with the energy gain or loss, as

$$F_j(\mathbf{q},\omega) = \left[\frac{n_{\mathbf{q}_j}(T) + \frac{1}{2} \pm \frac{1}{2}}{\omega_j(\mathbf{q})}\right] \delta(\omega \mp \omega_j(\mathbf{q})). \quad (13)$$

This homogeneous broadening is expected to be weak for the monolayer modes below 10 meV, but it can significantly increases in the case of a strong coupling with the bulk substrate modes. The single cause of broadening, which will be considered here, is due to the instrumental resolution (around 0.35 meV). The peak width will therefore be obtained by convoluting Eq. (10) with a triangular function.

IV. RESULTS AND DISCUSSION

A. Numerical results

1. *Determination of the dynamical solutions*

The solutions of the system of equations in Eq. (6) are determined according to the following procedure. In a first step, we multiply all the terms by $M(\omega^2, \mathbf{q})$ defined in Eq. (8) and formally write the determinant to be solved as

$$\det|M(\underline{d} - \underline{I}\omega^2) - \underline{\Gamma}^2\underline{G}^0\underline{\Delta}^2| = 0. \quad (14)$$

When the couplings vanish ($\underline{\Gamma}^2, \underline{\Delta}^2 = \underline{0}$), the 13 solutions of Eq. (14) are easily obtained as the three trivial roots of M and the ten eigenvalues ω_j^0 of $\underline{d}$ for each $\mathbf{q}$ value. The substrate modes are determined by using the values $c_\ell = 5114$ m s^{-1} and $c_t = 2453$ m s^{-1} calculated from the elastic constants given in Ref. 18. The density of matter of the continuum substrate is $\rho = 2210$ kg m^{-3}. The eigenvalues ω_j^0 are calculated[11] from the diagonalization of $\underline{d}$. In the second step, we consider the coupling terms, which depend on ω^2. As a consequence, the solutions of Eq. (14) cannot be determined from a diagonalization technique but by the calculation of the 13 roots of the determinant. When the coupling $\underline{\Gamma}^2\underline{G}^0\underline{\Delta}^2$ gets stronger compared to the $\underline{d}$ matrix, the solutions $\omega_j(\mathbf{q})$ are shifted from ω_j^0.

Examination of the elements of this latter matrix shows that the diagonal terms $d_{\alpha\alpha}$ are dominant and very similar for the two molecules, since the difference does not exceed 10%, indicating that the adsorption sites give nearly equal force constants, although the molecular orientations are different. The high values of the diagonal force constants, mainly for the z motion of the molecular centers of mass and for the θ and ϕ librations of the axes, are consistent with sharp potential wells. The nondiagonal elements $d_{\alpha\beta}$ ($\alpha \neq \beta$) are, in general, one order of magnitude smaller than the diagonal terms. However, some couplings can be significantly larger; these largest couplings imply either parallel modes x, y, and ϕ or perpendicular modes z and θ. Indeed, since the equilibrium orientation of the monolayer molecules is nearly flat above the surface, the θ motions contribute mainly to perpendicular modes, whereas the ϕ motions rather to parallel modes. Moreover, the matrix elements $\Gamma_{\alpha\gamma}^2$ and $\Delta_{\gamma\alpha}^2$ of the monolayer-substrate couplings decrease when the depth z of the substrate volume element increases. The maximum values for the couplings are thus determined[21,22] for the element at the surface ($z \to 0$), and they are, in general, smaller or similar to the nondiagonal terms $d_{\alpha\beta}$. The strongest couplings are in fact obtained between the perpendicular modes of the substrate surface and the perpendicular motions z and θ of the CO_2 molecules. The nondiagonal terms $d_{\alpha\beta}$ and the adsorbate-substrate couplings are responsible for the avoided crossing phenomena and hybridization of the dispersion curves with polaritonlike behavior at the resonances.[26]

The corresponding solutions for the displacements $\mathbf{u}(s)$ of the monolayer are then determined by replacing the solutions of the general determinant $\omega_j(\mathbf{q})$ into Eq. (6). For the substrate displacements $\mathbf{u}'(z)$, we use the calculated values of $\mathbf{u}(s)$ to solve Eq. (9). The final values $\mathbf{W} = \binom{\mathbf{u}}{\mathbf{u}'}$ can then be introduced into Eq. (12) to estimate $P_{ss'}$ or equivalently the spectral density function for the phonon-libron pairs of the system.

Before discussing the results, it may be interesting to analyze the implication of the approximations on the dynamical solutions. A numerical fit based on a mean-square procedure is used to determine the force constants occurring in the $\underline{d}$ matrix. The cutoff of the range of

radial and angular displacements in the fit is chosen in order to ensure an accuracy in the force constant values of better than 5%.[11] By assuming that the substrate is an isotropic continuum, we disregard the influence of the surface on the bulk frequency distribution, which could be easily taken into account in the slab model technique.[27] However, as we are mainly concerned with the coupled dynamics of the monolayer and substrate Rayleigh modes, such an assumption appears to be quite licit. A third approximation concerns the modification of the substrate vibrations due to the monolayer adsorption; such an effect has been discussed elsewhere,[20] and it is shown to remain negligible for a physisorbed system, excepted in the close neighborhood of the Γ point in the Brillouin zone. Let us finally mention that the mean force constants describing the adsorbate-substrate dynamical coupling can be overestimated when compared to a quite discrete model. This inaccuracy, which can reach 20% on some terms, could significantly increase the splitting of the hybridized dispersion curves due to avoided crossings, but it does not change the whole aspect of the curves.

2. *Dispersion relations*

Figure 2 displays the dispersion curves calculated from Eq. (14) when the wave vector **q** is along the ⟨110⟩ direction chosen for the experimental measurements. This direction is not equivalent for the two domains A and B rotated by 90° (cf. Fig.1), and as a consequence the Brillouin zone (BZ) associated with domain A is half the BZ for the domain B. Ten dispersion curves labeled A_1,...,A_{10} (B_1,...,B_{10}) correspond to the monolayer modes disturbed by the substrate dynamics. The three curves with increasing slope characterize successively the Rayleigh, transverse, and longitudinal bulk acoustic branches of the substrate.

The dispersion curves A_i and B_i for each value i are degenerated at the Γ point of the BZ; then the degeneracy is removed for $q \neq 0$ due to the anisotropy provided by the two types of domains. The ten curves A_i (B_i) are the result of a splitting by two of the motions of each molecule due, on one hand, to the fact that the adsorption sites $s = 1$ and 2 are not strictly equivalent and, on the other hand, to the coupling between the two molecules in the unit cell. Such a splitting is thus present even at $q = 0$. Two branches A_1 and A_2 (B_1 and B_2) have a quasiacoustic behavior with an energy gap at the Γ point, which characterizes the substrate corrugation viewed by the monolayer dynamics. They are assigned to parallel (x, y) translations of the molecular centers of mass with nevertheless a significant hybridization with the perpendicular modes z of the layer and of the substrate. The optical branches A_3,...,A_{10} (B_3,...,B_{10}) are more or less dispersive and range between 5 and 14 meV. They exhibit strong avoided crossing behavior, indicating that the nondiagonal elements of the $\underline{d}$ matrix play a significant role in the shape of the branches. The 10 dispersion curves A (B) are, furthermore, hybridized with the substrate branches and additional avoided crossings, although weak because of the small coupling tensors $\underline{\Gamma}^2$

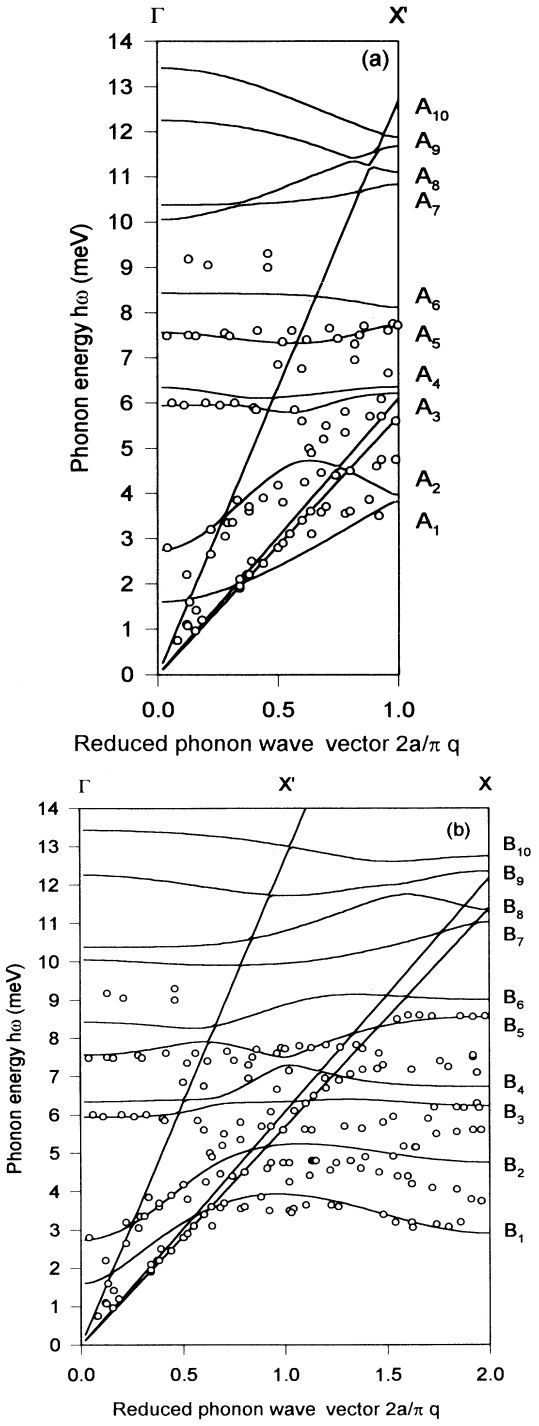

FIG. 2. Dispersion curves of the CO_2 monolayer $\hbar\omega$ vs $q^* = \frac{2a}{\pi}q$ (a) for domain A and (b) for domain B. Full curves correspond to the calculations, while empty circles are experimental data.

and $\underline{\Delta}^2$, are clearly evidenced in Figs. 2(a) and 2(b). The optical branches can be classified according to the following scheme. The A_3 and A_4 (B_3 and B_4) curves with energies around 6 meV are the result of the hybridization between y, z, and θ motions. The curves A_5 and A_6 (B_5 and B_6) around 8 meV are mainly assigned to z and θ

monolayer motions. The remaining branches A_7,...,A_{10} (B_7,...,B_{10}) for energies larger than 10 meV correspond rather to x and ϕ monolayer vibrations.

When the picture of the dispersion curves given in Fig. 2 is compared to that obtained within the rigid substrate approximation,[11] we can note two main differences. The first is connected to the modification of the shape of the branches at the resonances with the substrate modes; this effect remains weak because the coupling terms with the bulk modes of the substrate are themselves weak. The second arises from an overall change of the quasiacoustical branches due to the privileged coupling of these monolayer modes with the substrate surface motions; the corresponding effect is a change of the zero wave-vector gap and an increased dispersion of the monolayer modes.

3. *Spectral density function*

In order to study the relative importance of the various modes in the scattering spectrum, we have drawn a modified version of Eq. (10), which retains only the weighted spectral density function, i.e., the terms in the brackets and the Dirac function occurring in the function F_j. Figure 3 displays the results connected to the two domains and for the two asymptotic situations S_1 and S_2. Let us note that we consider only the energy loss side to be consistent with experimental results[7] and disregard the broadening; the apparent width of the resonance peaks corresponds to the numerical energy resolution in the calculation of the density function. We clearly see three energy regions in the spectral density function for both domains and both situations. In region I, in the upper -5 meV range, the density function exhibits either resonance peaks or, on the contrary, wider structures depending on the domain type and probe analysis. These signals are assigned from Fig. 2 to quasiacoustic branches A_1, A_2, B_1 and B_2, which are more or less dispersive depending on the q values. Region II, for energies ranging between -5.5 and -9.5 meV, corresponds to the weakly dispersive optical branches A_i, B_i ($i = 3$–6), and it displays sharp resonance peaks reflecting this small dispersion along the BZ. The signals in region III, beyond -10 meV, appear to be less resolved, and they can be assimilated to a more or less structured and wide band resulting from the more intricate shape of the dispersion curves A_i, B_i ($i = 7$–10).

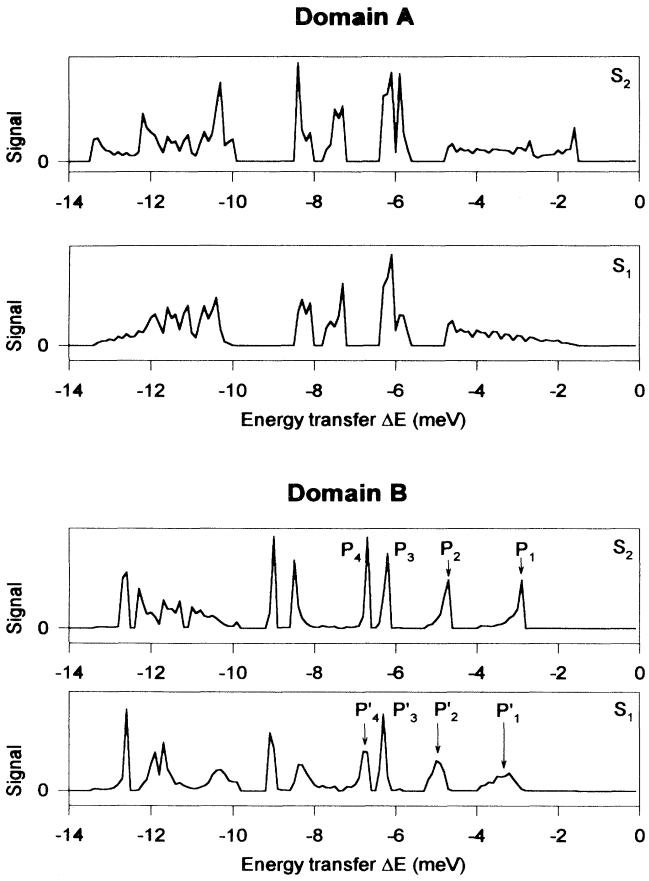

FIG. 3. Spectral density function (arbitrary unit) vs energy transfer for the CO_2 monolayer. Top: for domain A; bottom: for domain B. The two situations S_1 and S_2 are drawn.

Comparison of the spectral density function for domains A and B shows that peaks associated with the first domain are, in general, wider, as a consequence of the largest $\mathbf{q}$ dispersion of the branches in the smallest BZ. Examination of the signals analyzed within the two asymptotic situations S_1 and S_2 evidences clearly significant differences regarding the peak behavior, since some peaks are not modified, while other resonances can disappear. To interpret such a behavior, let us consider, for instance, the peaks labeled from P_1 to P_4 in domain B (Fig. 3) and analyze them in the light of the polarization factor $E_\perp$, defined as

$$E_\perp = \left[\frac{\mathrm{Re}\sum_{ss'} W_z^*(s')W_z(s)}{\mathrm{Re}\sum_{ss'} \mathbf{W}^*(s')\cdot\mathbf{W}(s)}\right]^{\frac{1}{2}}. \tag{15}$$

This factor describes the ratio of the perpendicular component of the displacement $\mathbf{W}$ [Eq. (12)] to the total displacement; Re defines the real part of the products occurring in the sum. Its behavior with $q^* = \frac{2\pi}{a}q$ is presented in Fig. 4 for the dispersion curves B_i ($i = 1,\ldots,4$) of domain B. Peak P_1' around -3.5 meV appears for the S_1 situation only, and it is assigned to the B_1 branch, which corresponds to a small dispersive perpendicular mode for $q^* > 0.8$, as shown by the value of the polarization factor. In the second situation S_2, peak P_1' is replaced by peak P_1, slightly less energetic (around -3 meV). P_1 can be assigned to the part of the acoustical B_1 branch that is more dispersive and clearly parallel, i.e., for $q^* < 0.8$ (Fig. 4). Since the intensity of P_1' is reduced by a factor 2 in situation S_2, as shown by the value of $E_\perp$ for B_1 (Fig. 4), it then occurs as a shoulder of P_1. A nearly similar phenomenon can interpret the strong decrease of the P_2' peak from situations S_1 to S_2 and the concomitant increase of the P_2 peak. Peak P_2 in situation S_2 is assigned to the B_2 branch, which is clearly parallel for $q^* \leq 0.8$, whereas the relative weights of parallel and perpendicular polarizations for the same branch are similar at larger q^* values, and they give rise

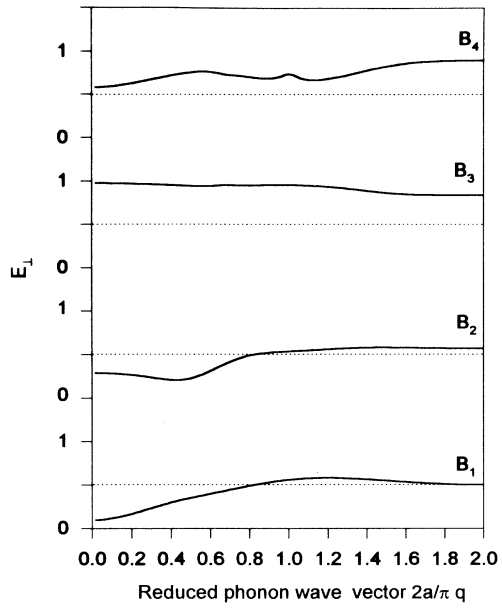

FIG. 4. Polarization factor $E_\perp$ [Eq.(15)] for the first four dispersion curves B_1–B_4 of domain B. A value $E_\perp = 1$ corresponds to a purely perpendicular polarization, while $E_\perp = 0.5$ defines an equally distributed parallel and perpendicular polarization.

to the P_2' peak for the S_1 situation.

The behavior of peaks P_3 and P_4, respectively, connected to the B_3 and B_4 modes is somewhat different from that of the previous peaks. Indeed, they occur in both situations with roughly similar intensities. The branches B_3 and B_4 are weakly dispersive (Fig. 4), and they give two intense signals around 6.5 and 7 meV in both situations. These branches have polarization factors, which vary in an opposite way, since $E_\perp$ decreases for B_3 and increases for B_4 when q^* increases. However, the variations with q^* of the polarization factor for B_3 have less incidence on the spectral density than for B_4, since B_3 remains mainly a perpendicular branch, while B_4 changes from a half perpendicular and half parallel nature to a nearly perpendicular one as q^* increases. As a result, the two peaks P_3 and P_4 appear in S_1 and S_2 at the same frequency. The intensity of peak P_3 is nearly the same for the two situations, whereas the intensity of peak P_4 is more sensitive to the polarization change. Similar arguments can be invoked to interpret the behavior of the other peaks in both domains.

Such an analysis of the spectral density function illustrates in a pertinent way the degree of accuracy we can hope for regarding the assignment of the frequencies of the vibrational modes of the layer and the interpretation of their dispersive behavior. It shows that hybridization of phonon-libron modes is particularly efficient to produce significant changes in the mode polarization. It is also a valuable test on the right sensitivity of the He scattering technique in probing selectively perpendicular or parallel polarized modes.

B. Comparison with experiments

The experimental data points corresponding to the pairs $(\hbar\omega, \mathbf{Q}_\parallel)$ are presented in Figs. 2(a) and 2(b). The points are deduced from the TOF spectra recorded[5,7] for various angles of incidence of the He beam with momentum transfer transformed to wave vector in the first BZ irrespective of the intensity modification due to BZ change. Moreover, experiments are unable to discriminate points that belong to domains A or B; therefore we have drawn the empty circles twice, in Figs. 2(a) and 2(b), although they each belong to a well-defined domain.

The agreement between data points and the quasi-acoustic curve B_1 is quite good for $q^* > 1$. At smaller q^* values, the hybridization between the A_1, B_1, and Rayleigh modes is well explained. Whereas the A_2 and B_2 modes at $q^* \leq 1$ are quite well taken into account by the experimental values, it seems that the B_2 mode at a larger q^* value is not dispersive enough, since an inaccuracy by 1 meV is observed at the X point of the BZ. Data points around 6 meV are clearly due to modes A_3 and B_3 up to the X' point and at the BZ limit (X point). The consistency is quite good for the undispersive A_5 and B_5 modes inside all the BZ. Data points around 9 meV are not interpreted but could be assigned to the A_6 and B_6 modes. It may be noted that the hybridization with the Rayleigh mode of both the acoustic and optic monolayer branches is well interpreted, since most of the points occurring outside the monolayer modes result from the coupling with the Rayleigh and bulk substrate modes. The main discrepancies are thus due to the too large energy of the B_2 and B_3 modes for $q^* > 1$, and they can be attributed to a weakness in the interaction potential accuracy.

However, as already mentioned, the data points can originate from different BZ's, and therefore we have to duplicate the BZ of domain A to describe the whole BZ of domain B. In that case, the A_2 and A_3 curves should be folded around X' in order to interpret the data points at $q^* > 1$. It is thus interesting to draw the scattering spectrum from the expression given by Eq. (10). The improvements with respect to Fig. 3 are the consideration of both the broadening due to instrumental resolution and the presence of two types of domains. The energy transfer spectra calculated with a resolution of 0.35 meV are presented in Fig. 5 for three different molar fractions of domains and compared to the experimental scattering spectrum[7] at 30 K for an angle of incidence θ_i equal to 43.5°. For this value of θ_i, most of the signals lie inside a single BZ, and no correction for scan curves must be considered.[28] The consistency seems to be better when the molar fraction of domains B is large, around 0.7 and 0.8, since most of the peaks are reproduced for energy values below 10 meV. All these peaks broadened by the experimental resolution can be easily assigned to the vibrational modes of the monolayer by examining Fig. 3. This clearly shows that the scattering spectrum depends on the domain presence. In contrast, this spectrum is poorly dependent on the He probe selectivity (situations S_1 and S_2) because the experimental broadening tends to mask the accurate frequency values of the peaks. Thus,

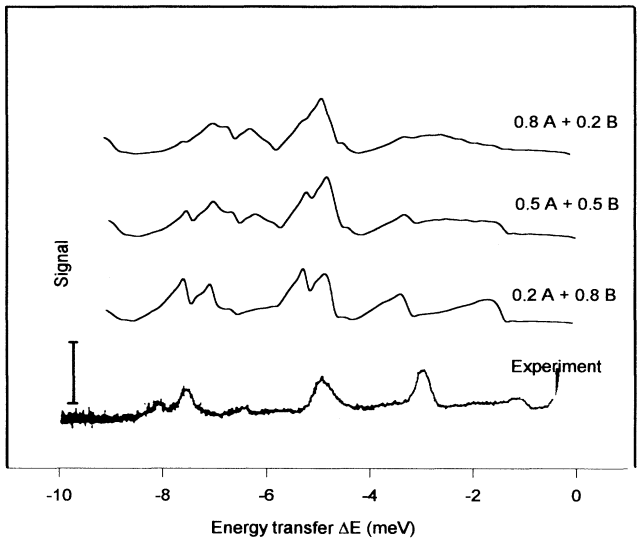

FIG. 5. Scattering spectrum (arbitrary unit) for the CO_2 monolayer. The three upper spectra are calculated with three different molar fractions of domains A and B. The experimental spectrum is issued from Ref. 7.

while it appears that the analysis of the spectral density functions can be extremely fruitful for the understanding of the probe selectivity vs mode polarization, the peak broadening prevents such an analysis using the energy transformed spectrum.

To our knowledge, this is the first time that such a detailed analysis of the low-frequency phonon-libron vibrational modes of a molecular monolayer physisorbed on a ionic substrate is performed. The present approach is obviously perfectible, since we have shown that improvements could be brought, on one hand, to a better description of the substrate and mainly of the couplings between the adsorbate and the substrate and, on the other hand, to the accuracy of the potential coefficients and to the consideration of correcting contributions. However, the overall agreement between experiments and calculations regarding the dispersion curves and the scattering spectrum is a test of the pertinency of the model. Indeed, it can be remarked that the molar fraction of domains A and B ($x_A = 0.2$ for A) used to bring the optimum consistency with the scattering spectrum is very close to that experimentally deduced from polarization infrared measurements for CO_2 on MgO(100) by Heidberg, Meine, and Redlich.[29] It agrees also with the value $x_A = 0.26$ deduced from our theoretical study[10] of the high-frequency vibrational modes (internal modes) for the same layer CO_2 adsorbed on NaCl(100). In this work, we use the same interaction potential to assign the infrared signals of the layer as in the present paper; the main difference is that the polarization infrared spectrum is characterized by the vibrational dependence of the potential instead of the translational and orientational dependences for the inelastic He scattering spectrum. The fact that the same potential form can be successful in interpreting results on the CO_2 monolayer adsorbed on NaCl issued from different experiments is a somewhat crucial argument of the model adequacy.

V. CONCLUSION

The dynamical properties of the CO_2 monolayer have been studied by developing semi–classical calculations up to the determination of the energy distribution spectrum, which can be compared to the experimental TOF scattering data. An extension of this study could be the analysis of the adsorbate-substrate dynamics for other He beam angles of incidence. Indeed, choosing a direction for $\mathbf{Q}_{\parallel}$, which is along a domain direction and perpendicular to the other domain type, naturally introduces the monolayer anisotropy. But probing with a 45° rotated He beam would partly restore the monolayer isotropy, and it could be interesting to verify such a property in experiments.

Moreover, the consideration of other adsorbates with different adsorption characteristics could provide additional understanding of the layer dynamics. In this way the phonons and librons of the stable (2×1) phase have been analyzed for the particular equilibrium configuration of the CO_2 molecule. Another system for which one has rich information on the equilibrium structure is the CO monolayer.[30,31] In that case, the molecular axes are rather perpendicular to the surface, still with librational motions. The mode polarizations associated with the angular motions would appear very different from the CO_2 situation for which the molecules are rather flat above the surface, and they should give rise to a different shape for the spectrum. The interaction potentials for CO adsorbed on NaCl(100) are at least as well known as those for CO_2, and calculations for this system would be straightforward when experiments are available.

ACKNOWLEDGMENTS

The Laboratoire de Physique Moléculaire is Unité associée au Centre National de la Recherche Scientifique No. 772.

[1] A.M. Bradshaw, Surf. Sci. **299/300**, 49 (1994); H. Ibach, *ibid.* **299/300**, 116 (1994); D. Menzel, *ibid.* **299/300**, 170 (1994).

[2] Y.J. Chabal, Surf. Sci. Rep. **8**, 211 (1988).

[3] H.J. Freund and E. Umbach, *Adsorption on Ordered Surfaces of Ionic Solids and Thin Films* (Springer, Berlin, 1993), Vol. 33.

[4] E. Hulpke, *Helium Atom Scattering from Surfaces*

(Springer, Berlin, 1992), Vol. 27.
[5] J. Heidberg, E. Kampshoff, R. Kühnemuth, O. Schönekäs, G. Lange, D. Schmicker, J.P. Toennies, R. Vollmer and H. Weiss, J. Electron Spectrosc. Relat. Phenom. **64/65**, 341 (1993).
[6] J. Schimmelpfennig, S. Fölsch, and M. Henzler, Surf. Sci. **250**, 198 (1991).
[7] G. Lange, J.P. Toennies, R. Vollmer, and H. Weiss, J. Chem. Phys. **98**, 10 096 (1993).
[8] G.Y. Liu, G.N. Robinson, G. Scales, and P.A. Heiney, Surf. Sci. **262**, 409 (1992).
[9] C. Girardet, S. Picaud, and P.N.M. Hoang, Europhys. Lett. **25**, 131 (1994).
[10] S. Picaud, S. Briquez, A. Lakhlifi, and C. Girardet, J. Chem. Phys. **102**, 7229 (1995).
[11] S. Picaud, P.N.M. Hoang, and C. Girardet, Surf. Sci. **322**, 381 (1995).
[12] J. Heidberg, E. Kampshoff, R. Kühnemuth, O. Schönekäs, H. Stein, and H. Weiss, Surf. Sci. Lett. **226**, L43 (1990).
[13] J. Heidberg, E. Kampshoff, R. Kühnemuth, and O. Schönekäs, Surf. Sci. **251/252**, 314 (1991).
[14] J. Heidberg, E. Kampshoff, R. Kühnemuth, and O. Schönekäs, Surf. Sci. **272**, 306 (1992).
[15] O. Berg, R. Disselkamp, and G.E. Ewing, Surf. Sci. **277**, 8 (1992).
[16] J. Heidberg, E. Kampshoff, R. Kühnemuth, and O. Schönekäs, J. Electron Spectrosc. Relat. Phenom. **64/65**, 803 (1993); *ibid.* Can. J. Chem. **72**, 795 (1994).
[17] S. Briquez, A. Lakhlifi, S. Picaud, and C. Girardet, Chem. Phys. **94**, 65 (1995).
[18] R.F.S. Hearmon in *Elastic, Piezoelectric, Piezooptic, and Electrooptic Constants of Crystals*, edited by K-.H. Hellwege, Landolt-Börnstein, New Series, Group III, Vol. 1 (Springer, Berlin, 1966), p. 30.
[19] L.D. Landau and E.M. Lifshitz, *Theory of Elasticity* (Pergamon, London, 1963).
[20] P.N.M. Hoang and C. Girardet, Surf. Sci. **243**, 361 (1991).
[21] P.N.M. Hoang and C. Girardet, Phys. Rev. B **44**, 1209 (1991).
[22] C. Girardet and P.N.M. Hoang, Surf. Sci. **282**, 288 (1993).
[23] V. Celli, G. Benedek, U. Harten, J.P. Toennies, R.B. Doak, and V. Bortolani, Surf. Sci. **143**, L376 (1984).
[24] D. Eichenauer and J.P. Toennies, J. Chem. Phys. **85**, 532 (1986).
[25] J.R. Manson, in *Helium Atom Scattering from Surfaces* (Ref. 4), p. 173.
[26] B. Hall, D.L. Miller, and J.E. Black, Phys. Rev. B **32**, 4932 (1985).
[27] F.W. De Wette, *Surfaces Phonons*, edited by W. Kress and F.W. De Wette (Springer, Berlin, 1991), Vol. 21, p. 67.
[28] G. Brusdeylins, R.B. Doak, and J.P. Toennies, Phys. Rev. B **27**, 3662 (1983).
[29] J. Heidberg, D. Meine, and B. Redlich, J. Electron Spectrosc. Relat. Phenom. **64/65**, 599 (1993).
[30] J. Heidberg, E. Kampshoff, and M. Suhren, J. Chem. Phys. **95**, 9408 (1991); D. Schmicker, J.P. Toennies, R. Vollmer, and H. Weiss, *ibid.* **95**, 9412 (1991).
[31] S. Picaud, P.N.M. Hoang, C. Girardet, A. Meredith, and A.J. Stone, Surf. Sci. **294**, 149 (1993).

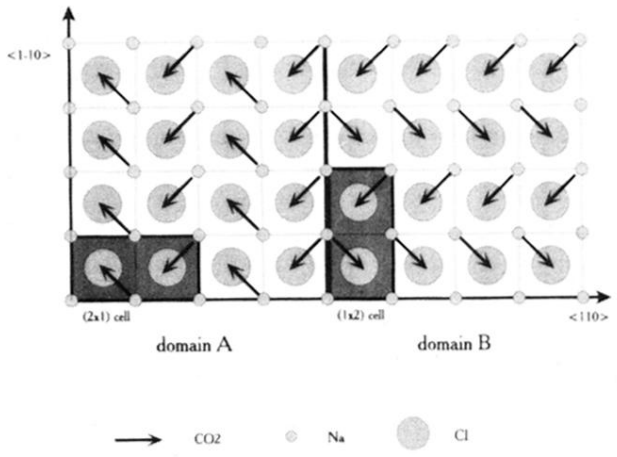

FIG. 1. Geometry of the (2×1) commensurate CO_2 monolayer adsorbed on NaCl(100). The two unit cells associated with domains A (left) and B (right) are represented by dark rectangles. The arrows indicate that the molecular axes are tilted upwards.